JOURNAL OF GEOPHYSICAL RESEARCH, VOL. 106, NO. E8, PAGES 17,683–17,698, AUGUST 25, 2001

Thermal and Evolved Gas Analyzer: Part of the Mars Volatile and Climate Surveyor integrated payload

William V. Boynton,[1] Samuel H. Bailey,[1] David K. Hamara,[1] Michael S. Williams,[1] Rolfe C. Bode,[1] Michael R. Fitzgibbon,[1] WenJeng Ko,[1] Michael G. Ward,[1] K. R. Sridhar,[1] Jeff A. Blanchard,[1] Ralph D. Lorenz,[1] Randy D. May,[2] David A. Paige,[3] Asmin V. Pathare,[3] David A. Kring,[1] Laurie A. Leshin,[4] Douglas W. Ming,[5] Aaron P. Zent,[6] D. C. Golden,[5] Kristopher E. Kerry,[1] H. Vern Lauer Jr.,[5] and Richard C. Quinn[6]

Abstract. The Thermal and Evolved Gas Analyzer (TEGA) on the Mars Polar Lander spacecraft is composed of two separate components which are closely coupled: a Differential Scanning Calorimeter (DSC) and an Evolved Gas Analyzer (EGA). TEGA has the capability of performing differential scanning calorimetry on eight small (0.038 mL) soil samples selected in the vicinity of the lander. The samples will be heated in ovens to temperatures up to 950°C, and the volatile compounds water and carbon dioxide, which are released during the heating, will be analyzed in the EGA. The power required by the sample oven is continuously monitored during the heating and compared to that required to heat simultaneously a similar, but empty, oven. The power difference is the output of the DSC. Both endothermic and exothermic phase transitions can be detected, and the data can be used in the identification of the phases present. By correlating the gas release with the calorimetry, the abundance of the volatile compounds associated with the different phases can be determined. The EGA may also be able to detect the release of oxygen associated with any superoxide that may be on the surface of the soil grains. The instrument can detect the melting of ice in the DSC down to abundances on the order of 0.2% of the sample, and it can detect the decomposition of calcite, $CaCO_3$, down to abundances of 0.5%. Using the EGA, TEGA can detect small amounts of water, down to 8 ppm in the sample, and it can detect the associated release of CO_2 down to the equivalent abundances of 0.03%. The EGA also has the ability to determine the $^{13}C/^{12}C$ ratio in the evolved CO_2, but it is not clear if the accuracy of this ratio will be sufficient to address the scientific issues.

1. Introduction

The Thermal and Evolved Gas Analyzer (TEGA) instrument (Plate 1) will perform calorimetry and evolved gas analysis on soil samples collected from the Martian surface. TEGA is one component of the Mars Volatile and Climate Surveyor (MVACS) integrated payload (see D.A. Paige et al., manuscript in preparation, 2001), designed specifically to explore the volatile and climate history of Mars from the unique perspective of a landing site near the southern pole. The other MVACS instruments include the stereo surface imager (SSI) [*Smith et al.*, this issue], the meteorological station (MET) (D. Crisp et al., manuscript in preparation, 2001), and the robotic arm (RA) [*Bonitz et al.*, this issue] with a robotic arm camera (RAC) [*Keller et al.*, this issue]. The MVACS payload is part of the Mars Polar Lander (MPL) Mission which was launched January 3, 1999, and had been scheduled to land on December 3, 1999 (see R.W. Zurek et al., manuscript in preparation, 2001).

The TEGA will accept soil samples excavated by the RA from depths up to 0.5 m. Prior to delivery to the TEGA, the samples will be photodocumented by the RAC and SSI. The TEGA instrument comprises two analytically distinct components: a thermal analyzer (TA), which will investigate phase transitions in the sample, and an evolved gas analyzer (EGA), which will quantify the amounts of water, carbon dioxide, and oxygen evolved from the sample as it is heated. The purpose of this paper is to describe the scientific rationale and approach of the TEGA experiment and to provide a detailed description of the instrument.

2. TEGA Science

The main science objectives of TEGA are to determine the abundances of the two climatologically most important volatile compounds in the Martian soil, water and carbon dioxide, and the minerals or phases with which they are associated. In addition, TEGA will also attempt to measure the isotopic ratio of carbon in the carbon dioxide and constrain the amount and nature of the putative strong oxidant found in the Martian soil by Viking.

[1]Lunar and Planetary Laboratory, University of Arizona, Tucson, Arizona.
[2]Jet Propulsion Laboratory, California Institute of Technology, Pasadena, California.
[3]Department of Earth and Space Sciences, University of California, Los Angeles, California.
[4]Department of Geology, Arizona State University, Tempe, Arizona.
[5]Johnson Space Center, Houston, Texas.
[6]Ames Research Center, Moffett Field, California.

Copyright 2001 by the American Geophysical Union.

Paper number 1999JE001153
0148-0227/01/1999JE001153$09.00

2.1. Soil and Polar Layered Deposits

The targeted landing site for the MPL is in the polar layered deposits, which are most often interpreted as sedimentary units whose deposition was influenced by fluctuating climatic conditions on the planet [*Thomas et al.*, 1992]. The layered terrain is extensive, covering areas as far south as 80° around the north pole and as far north as 70° around the south pole. The Mars Orbiter Laser Altimeter measurements of the north polar region suggest that the stratigraphic thickness is 1.03 km on average with a maximum thickness of 2.95 km [*Zuber et al.*, 1998]. The deposits in the south polar region have a similar thickness [*Smith et al.*, 1999].

Viking orbital images and thermal inertia maps show that the surface of the south polar layered deposits is mantled with a layer of fine bright dust of unknown depth [*Herkenhoff and Murray*, 1990; *Paige and Keegan*, 1994]. Surface dust on Mars is both ubiquitous and mobile, and it is expected that the dust deposit on the south polar layered deposits is characteristic of dust deposits elsewhere on the planet.

In addition to samples of surface dust, TEGA may also analyze subsurface materials from the polar layered deposits. These deposits, which are described in greater detail by *Vadavada et al.* [2000] are believed to be an admixture of water ice, dust, and sand. At the present time, we have few constraints on the origin and evolution of these deposits. TEGA analyses should provide a first-order view of the amount of water and carbon dioxide in the uppermost layers of the deposit at the landing site as well as their variations in composition to a depth of 0.5 m below the surface.

2.2. Reservoirs of Water and Carbon Dioxide

One of the potential soil reservoirs of water is ice. Theoretical models that take into account the thermal inertia and albedo of the soil, the abundance of water in the atmosphere, effects of water vapor diffusion and absorption in the soil, and past changes in Mars orbital elements predict that significant regions of the planet could have stable ice within 0.5 m of the surface [*Zent et al.*, 1986; *Paige*, 1992; *Mellon and Jakosky*, 1993]. This ice could represent a significant fraction of the Martian water budget.

Another important potential reservoir is the collection of minerals that comprise the Martian soils. Analysis of the volatile content of Martian soils, with knowledge of the phases in which the volatiles reside, will provide significant tests of hypotheses concerning past climate on Mars. If the soils contain crystalline clay minerals and abundant carbonates, it will suggest a past climate in which water was present for long periods. On the other hand, poorly crystalline clay minerals with little carbonate would indicate only brief periods of water interactions [*Gooding et al.*, 1992a, 1992b, 1994]. A list of volatile-containing minerals that past studies suggest could be in the soils at the MPL landing site has been compiled in Table 1. Most of these minerals have reactions that can be recognized by TEGA. These reactions include dehydration (e.g., when kieserite, $MgSO_4 \cdot H_2O$, loses its bound water), dehydroxylation (e.g., when lepidocrocite, γ-FeOOH, loses OH to form maghemite), decarbonization (e.g., when magnesite, $MgCO_3$, loses CO_2 to form periclase, MgO), and structural changes (e.g., when Fe_2O_3 is converted from the gamma form, maghemite, to the alpha form, hematite).

In addition to ice and chemically combined volatiles, there may be sites in the soils for adsorbed volatiles. Laboratory experiments [*Mooney et al.*, 1952; *Fanale and Cannon*, 1971, 1974, 1978; *Anderson et al.*, 1978; *Zent et al.*, 1987; *Zent and Quinn*, 1995] and models [*Toon et al.*, 1980; *Fanale et al.*, 1982; *Zent et al.*, 1987; *Francois et al.*, 1990; *Zent and Quinn*, 1995] have shown that both H_2O and CO_2 can be adsorbed by candidate Mars regolith materials and that this adsorptivity is a strong function of temperature and pressure [*Fanale et al.*, 1982]. Published estimates for the true sizes of the adsorbed H_2O and CO_2 reservoirs vary widely because of uncertainties in the adsorptive properties of the regolith materials, their physical states, and the extent of the regolith itself [*Carr*, 1986; *Fanale and Cannon*, 1971; *Fanale et al.*, 1982; *Clifford*, 1984]. However, most workers agree that the present Martian inventory of H_2O and CO_2 probably exceeds the present atmospheric inventory by up to 2 orders of magnitude. These same workers also agree that because of its lower annual average temperature, the near-surface high-latitude regolith is by far the most likely location for significant adsorbed CO_2 and H_2O reservoirs [*Clifford and Hillel*, 1983; *Fanale et al.*, 1986, 1992].

2.3. CO_2 Isotopic Composition

Light-element stable isotopes are tracers of the interactions between different volatile reservoirs and of the physical processes that shape those reservoirs. In terrestrial laboratories, carbon and oxygen isotopic studies of CO_2 released from bulk Martian samples (in the form of Martian meteorites) have produced valuable insights into Martian geologic processes and environmental conditions [e.g., *Carr et al.*, 1985; *Clayton and Mayeda*, 1988; *Jull et al.*, 1995; *Leshin et al.*, 1996; *Romanek et al.*, 1994; *Wright et al.*, 1986, 1992]. Of particular interest in this case are prior studies of CO_2 released from samples heated under vacuum [e.g., *Carr et al.*, 1985; *Leshin et al.*, 1996; *Wright et al.*, 1986, 1992] because those experiments are quite analogous to those that will be performed on Mars by TEGA. These studies suggest the presence of three main carbon-bearing components in SNC meteorites, distinguished by their temperature of release and their isotopic composition. The three components are a low-temperature component, which probably represents terrestrial contamination, a middle-temperature component, produced by the breakdown of Martian carbonate, and a high-temperature component, representing either the release of Martian magmatic volatiles or further terrestrial contamination. The variation in $^{13}C/^{12}C$ of these three components can be as much as 7% in a single meteorite. The carbonate component is interesting because it is variable in isotopic composition ($^{13}C/^{12}C$ of this component varies by ~4% from meteorite to meteorite), probably reflecting differences in the source of fluids from which the carbonates formed (e.g., the fraction of meteoric versus magmatic components in these fluids) or the variation of isotopic composition of the meteoric component with time due to variations in atmospheric isotopic composition.

2.4. Soil Oxidant

The Viking landers provided evidence that the Martian regolith is highly reactive and may exhibit strongly oxidizing properties. Oxygen was released in the Gas Exchange Experiment and from added radioactive organics in the Labeled Release (LR) Experiment. The most common hypotheses to explain these results invoke multiple oxidizing species [*Klein*, 1978] likely derived from the photolysis of water vapor in the atmosphere [e.g. *Zent and McKay*, 1994]. The abundance of the putative oxidants is on the order of a few tens of ppm and is compatible with the oxidants being on grain surfaces.

Table 1. Typical Potential Minerals at the Mars Polar Lander Landing Site, Relevant Major Reaction Enthalpies, and the Temperatures at Which They Occur[a]

Mineral Type, Name	Chemical Formula	T (K) of Reaction	Type of Reaction	ΔH, J/g	Comments	Reference[b]
Oxides						
Lepidocrocite	γ-FeOOH	473-633	dehydration γ-FeOOH→γFe_2O_3	240	endotherm H_2O evolved	5
Maghemite	γ-Fe_2O_3	690-773	Maghemite→Hematite	-77	exotherm	4
Pyrolusite	MnO_2	813-953	Pyrolusite→Mn_2O_3	1130	endotherm O_2 release	2,4
6L-Ferrihydrite	$5Fe_2O_3•9H_2O$	430-490	dehydration	246	endotherm H_2O evolved	2,4
		473-773	crystallization		sharp exotherm	2
Goethite	α-FeOOH	493-673	dehydration	275	endotherm H_2O evolved	4
Clays						
Chrysotile	$Mg_3Si_2O_5(OH)_4$	420	dehydration		H_2O evolved	2
		873-983	dehydration (structural)		H_2O evolved	2
		1100-1120	Forsterite recrystallization		sharp exotherm	2
Serpentine	$Mg_2Si_2O_5(OH)_4$	373-393	dehydration		H_2O evolved	2
		883-983	dehydration (structural)		large endotherm	2
		1083-1113	Enstatite recrystallization		sharp exotherm	2
Nontronite	$Fe_2(Al,Si)_4O_{10}(OH)_2Na_{0.3}•4H_2O$	398-523	water desorption	84-126	H_2O evolved	3
		673-873	dehydroxylation	105-168	H_2O evolved	3
		1070	structural change			
Montmorillonite	$(Al,Mg)_8(Si_4O_{10})_3(OH)_{10}•12H_2O$	398-533	dehydration	0-168		2,3
		898-1023	dehydration	96-252		2,3
		1073-1198	dehydration	42-84		2,3
		1173-1253	dehydration	42-126		2,3
Talc	$Mg_3[(OH)_2Si_4O_{10}]$	1073-1323	dehydration (structural)	210-336	H_2O evolved	2,3
Illite	$(K,H_2O)Al_2(H_2O,OH)_2.AlSi_3O_{10}$	423-473	dehydration	0-42	H_2O evolved	3
		773-923	dehydration	105-210	H_2O evolved	3
		1123-1193	Al^{3+}, Mg^{2+}, Fe^{3+} exchange	0-21	endo+exotherm	3
Carbonates						
Aragonite	$CaCO_3$	793-803	Aragonite→Calcite		small endotherm	2
Calcite	$CaCO_3$	1067-1177	decarbonation →CaO	1675	CO_2 evolved	2
Hydromagnesite	$(Mg_5(CO_3)_4(OH)_2•4H_2O)$	460-543	dehydration	363	endotherm H_2O evolved	4
Magnesite	$MgCO_3$	773	crystallization of MgO	-185	sharp exotherm	2,4
		867-897	decarbonation	1710	large endotherm. CO_2 evolved	2,4
Ankerite	$Ca(Fe,Mg,Mn)(CO_3)_2$	973-993	change in crystal structure		large exotherm	2
		1120-1200	decomposition		endotherm CO_2 evolved	
Siderite	$FeCO_3$	773	decomposition	715-1763	endotherm CO_2 evolved	2,4
Sulfates						
Epsomite	$MgSO_4•7H_2O$	320	stepwize dehydration → Kieserite		H_2O evolved	2
Kieserite	$MgSO_4•H_2O$	610	dehydration		H_2O evolved	2
Melanterite	$FeSO_4•7H_2O$	360	dehydration→Rozenite		H_2O evolved	
		960	decomposition		SO_2 and SO_3 evolved	
Gypsum	$CaSO_4•2H_2O$	350-440	dehydration	625	endotherm H_2O evolved	2,4
Anhydrite	$CaSO_4$	610-670	transition to insoluble form		small endotherm	2
Thennardite	Na_2SO_4	485-516	polymorphous transformation		large endotherm	2
		1158	fusion		large endotherm	2
Arcanite	K_2SO_4	856	phase transformation	48.6		1
Jarosite	$KFe_3(SO_4)_2(OH)_6$	573-673	decomposition to K_2SO_4• $Fe_2(SO_4)_3$		medium endotherm	2
		923-705	decomposition of $Fe_2(SO_4)_3$		medium endotherm	2
Halides						
Halite	NaCl	1070	fusion	481		1
Sylvite	KCl	1040	fusion	352		1

[a]Positive ΔH values indicate endothermic transitions. Note that reactions that typically occur in terrestrial laboratory analyses in air (e.g., Pyrite oxidation) are not shown, nor are transitions above 1200 K. The list of clays is illustrative but not exhaustive.

[b]References: 1, calculated from *Robie et al.* [1978]; 2, from the compilation of *Blazek* [1972]; 3, from *de Bruyn and van der Marel* [1954]; 4, our own experiments; 5, *Golden et al.* [1999].

Although H_2O_2, a plausible oxidant, is unlikely to diffuse to depths greater than a few centimeters, the regolith is known to be oxidizing to depths of at least 10 cm. Therefore either physical mixing of the oxidized soil material has taken place, or diffusion of another species is responsible [*Zent*, 1998]. The TEGA will attempt to measure O_2 release as a function of temperature in samples from a variety of depths in order to characterize the decomposition temperature, which is an important clue to the chemical composition of the oxidant.

3. Basis of Technique

TEGA is well suited to analyze the important volatile constituents water and carbon dioxide. It combines two instruments, a thermal analyzer and an evolved gas analyzer, to make a synergistic analysis of the amount of volatiles in the soil and the mineral phases with which they are associated.

The eight thermal analyzers that compose TEGA are differential scanning calorimeters (DSC), each of which has two

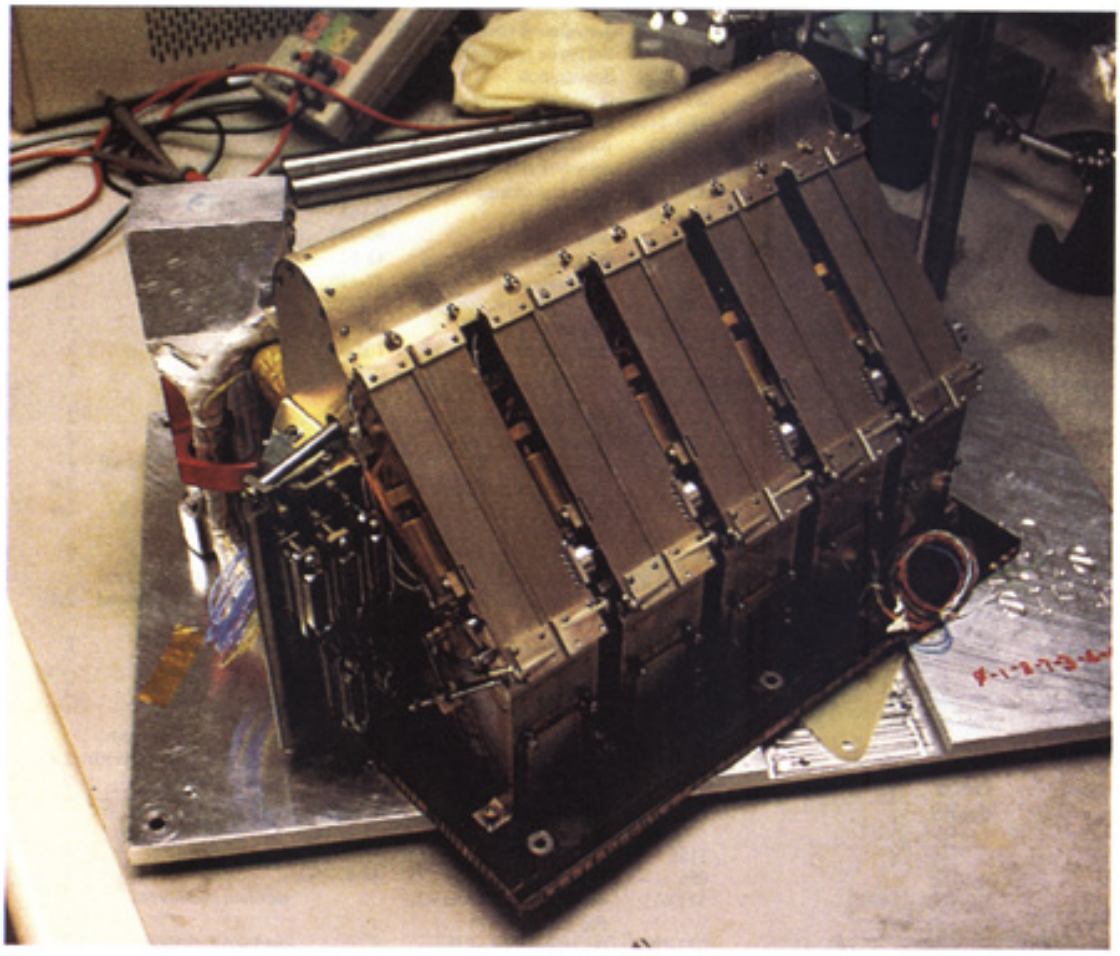

Plate 1. Flight model of the Thermal and Evolved Gas Analyzer. Five of the eight one-use thermal analyzer modules are visible. The carrier and calibration gas tanks, gas handling system, oxygen sensor, diode-matrix switching board, and wiring management system are housed between the bank of five thermal analyzers shown and the bank of three analyzers not in view on the opposite side of the instrument. The tunable diode laser spectrometer is on the left in a separate housing with its cover removed. For scale, each thermal analyzer module is 38 mm wide.

ovens: one contains the sample, and the other, a reference oven, is empty but is otherwise identical to the sample oven. The two ovens are heated concurrently according to a programmed temperature ramp, and the heat to maintain both ovens at the ramp temperature is monitored. To the extent that the ovens are truly identical in both their heat capacity and thermal losses to the environment, the difference in heat required by the sample and reference is attributed to that needed to heat the sample at the commanded temperature ramp. The output of the instrument is simply the differential heat flow to the two ovens plotted as a function of time (or temperature).

When a phase transition occurs, the enthalpy associated with the transition will be noted in the differential output. If the transition is endothermic, for example, the melting of ice, the heat required to effect the melting, 334 J/g, will be added to the sample oven as the sample is heated past the ice melting point. This heat is in addition to that required by the heat capacity of the sample and results in a positive peak in the differential output. In contrast, if there is an exothermic transition, the sample will require less heat than otherwise, and a negative peak in the differential output will be observed. In both cases the area of the peak is equal to the enthalpy (ΔH) of the reaction.

While the sample is being heated, a carrier gas of N_2 is passed through the ovens to transport any evolved gases to the EGA. The EGA continuously monitors the gas stream, and the output is time correlated to the DSC output in order to associate gas release with any observed phase transitions.

The EGA consists of two in-line cells; the first has an oxygen sensor, and the second is a Herriott cell for a tunable-diode laser (TDL) spectrometer which determines CO_2 and H_2O abundances. The oxygen sensor is based on an yttria-doped zirconia electrolyte in which the current is proportional to the partial pressure of oxygen. The TDL spectrometer has two lasers, one for CO_2 and one for H_2O, the output of which make multiple passes through the gas to increase the path length to 1.00 m. After passing through the gas, the laser output is detected via a photodiode. The wavelength of the laser is scanned over a narrow range to determine the infrared absorption of the lines of interest.

4. Instrument Description

TEGA is composed of three main components: the main electronics, which reside in the payload electronics box (PEB), the auxiliary electronics box (AEB), which contains sensitive front-end electronics that are located close to the instrument to reduce noise, and the sensor head. The sensor-head includes (1) eight single-use thermal analyzer modules to receive soil samples and perform differential scanning calorimetry (DSC) over the temperature range of Mars ambient to 950°C, (2) a gas-handling system to distribute and control carrier or calibration gas, (3) an oxygen sensor to detect evolved oxygen, and (4) a tunable-diode laser (TDL) spectrometer to determine the amount of water vapor and carbon dioxide evolved from the DSC ovens.

TEGA is a complex instrument, the mechanical components of which have been described in more detail elsewhere [*Williams et al.*, 1998]. It contains 36 valves and actuators (9 wax motors, 8 solenoids, 19 valves) and 83 moving parts. In addition to the ovens, it contains 15 separately regulated heaters for thermal control (8 upper tee, manifold and plumbing, TDL blanket, analog electronics box (AEB), 2 TDL lasers, calibration-gas tank, and oxygen sensor), in addition to the 16 heaters and temperature sensors associated with the ovens. TEGA has a mass, including cables and payload electronics box (PEB) electronics boards, of 5.71 kg. Its power requirements vary as a function of ambient temperature, the mode in which it is operating, and the temperature of the ovens. It ranges from 9.6 W in quiescent mode with all heaters off to a maximum of 78.0 W at maximum oven power with all heaters operating. A block diagram of TEGA is shown in Figure 1.

4.1. Thermal Analyzers

The sensor head contains eight single-use thermal analyzer modules. Each module (Figure 2) incorporates doors to prevent cross contamination of the module from soil loading of adjacent modules, a soil-processing system, reference and sample calorimetry ovens, and an oven-closure mechanism. The gas-handling system stores and controls the release of carrier gas and calibration gas, regulates the pressure and flow of the selected gas, distributes the gas to the selected thermal analyzer module, and directs evolved gases to the evolved gas analyzer.

Each module has two doors attached by spring-loaded hinges to the sides of the module. While closed, the doors overlap to create a seal against particulate contamination. After the doors are opened, an extension on the open door forms a dam to hold back the flow of soil.

The door latch is released by a clutched axle attached to a solenoid. A memory-metal (Nitinol) release inhibits the clutch from any advance until a release temperature (-25°C ± 5°C) is achieved. This feature was included to prevent the doors from inadvertently opening as the result of vibration experienced during launch.

The soil-processing system receives soil from the robotic arm and transports soil to the sample oven. Soil will fall from the robotic arm onto a slanted screen with a 1-mm grid. Fines falling through the grid enter a funneled path leading to a 2.5-mm transfer port. Astride the port is a three-bladed miniature soil impeller mounted on a wire. The wire is driven by the door-latch solenoid, which is excited at a ramped frequency causing the impeller to spin. As it spins, the impeller sweeps particles to the hole and imparts a vibration to the module chassis to encourage soil to advance toward the transfer port. The wire extends into the hole and agitates the soil particles to prevent bridging.

A light-emitting diode (LED) and detector pair are located across the throat of the soil-loading hole. Particles falling through the hole are detected as they occlude the light. This signal is integrated to give a positive indication of a successful soil load.

The correlation with amount in the oven and output of the integrator is not adequate to quantitatively determine the amount of soil in the oven, but it does serve as a flag to make it less likely that we would autonomously close an empty oven on Mars. In many cases a full oven has the light from the LED totally blocked by soil in the soil-loading hole.

The male portion of the sample calorimeter oven is stationed at the exit of the transfer port where it receives the sample. It consists of a tapered nickel cylinder supported by a thin-walled stainless steel carrier-gas inlet plumbing line (Figure 3). Nickel was chosen for its limited chemical reactivity and its high thermal conductivity. Thin-walled stainless-steel tubing was selected to minimize the conductive heat loss. The female portion of the oven is mounted to the housing at an angle to receive the male taper and includes heating and temperature-sensing windings.

The heating and temperature-sensing oven windings are 0.075 mm and 0.05 mm, respectively, platinum wires, solenoidally bi-filar wound about the female body. The temperature-sensing wire

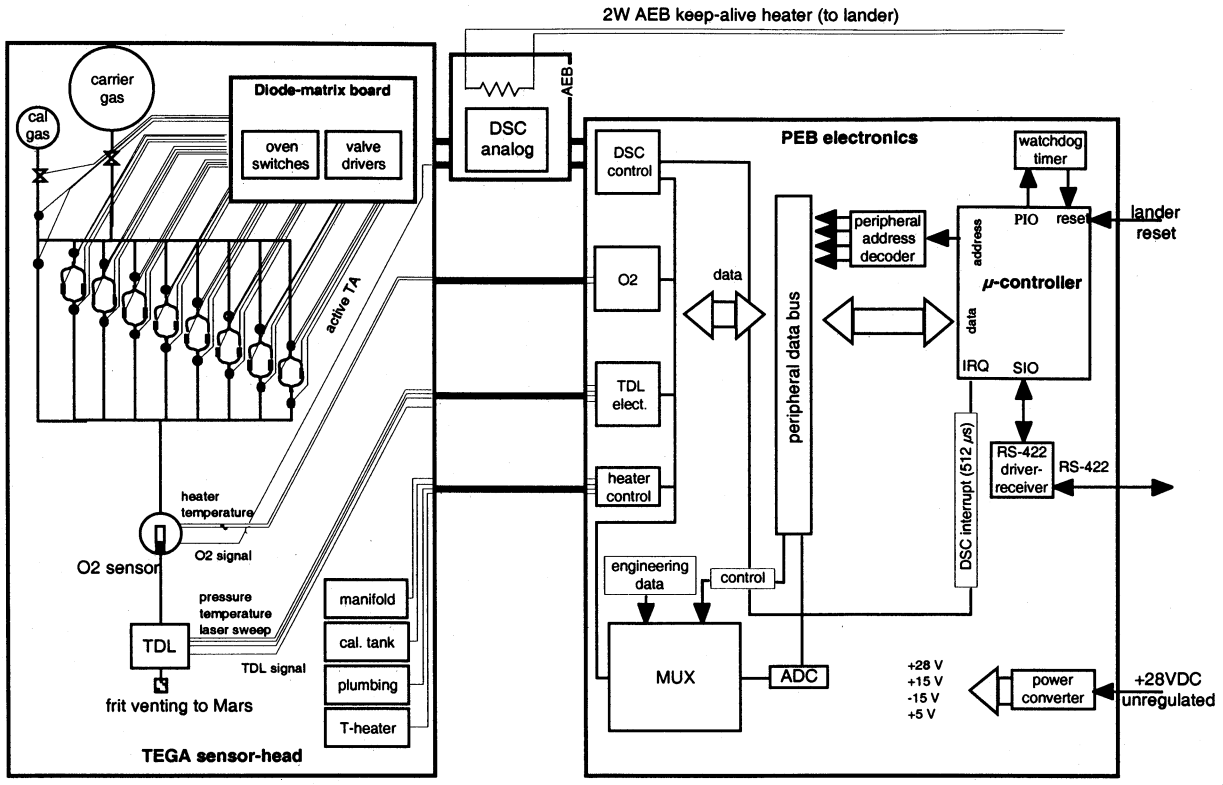

Figure 1. TEGA instrument block diagram. The functions of the TEGA sensor head are controlled by the electronics located in the warm Payload Electronics Box (PEB). The low-level analog signals are amplified in the analog electronics box (AEB) located near the sensor head.

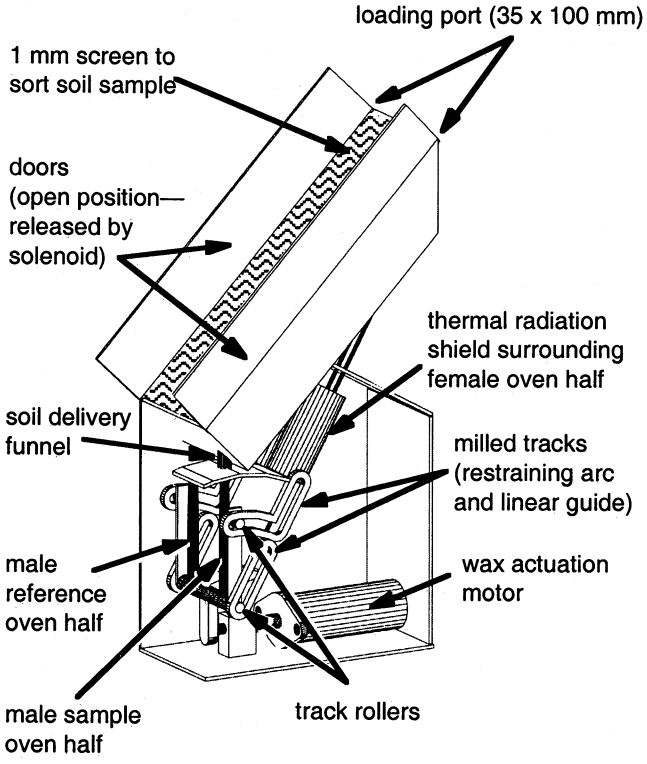

Figure 2. Cut-away schematic of thermal analyzer module illustrating the principal mechanical components. Each module includes a total of about 100 parts. The module receives the sample from the robotic arm, directs it into the male sample oven half, seals the ovens, and provides the plumbing for carrier-gas flow to and from the ovens. The wax motor rotates the two male ovens to bring them into alignment with the female oven halves. A spring then joins the oven halves, making a gas-tight seal. TEGA has eight of these one-use modules.

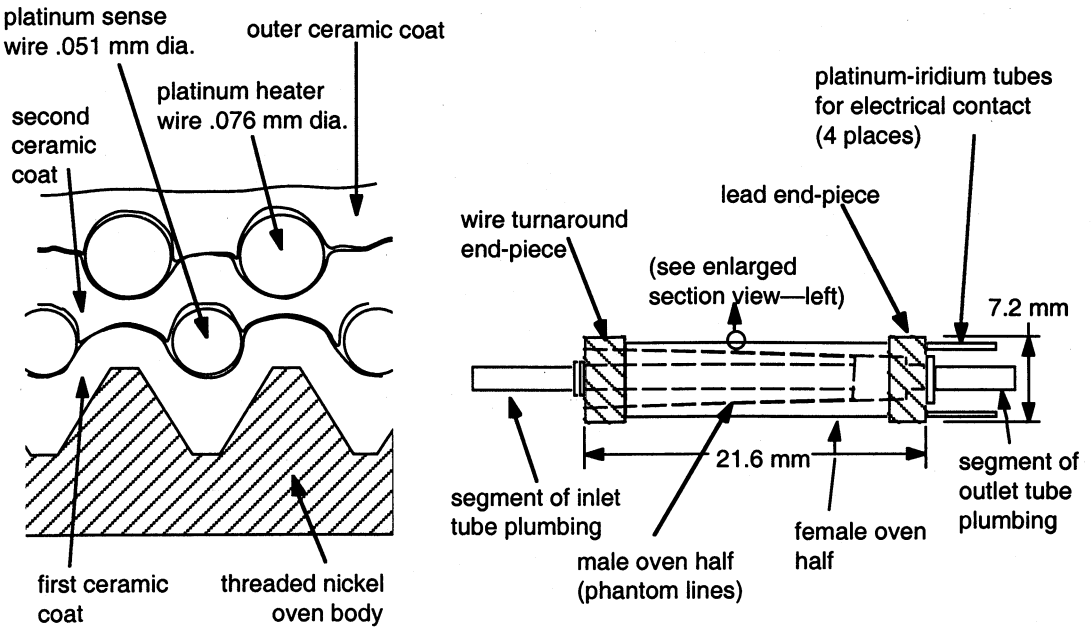

Figure 3. Schematic of TEGA oven construction. The sample oven volume is ~38 μL. The sample is loaded into the male oven half, which is then inserted into the female half to make a gas-tight seal, as seen in the lower view. The top cut-away view shows a cross-section enlargement of the temperature sense wire and heater wires with their ceramic insulation. The temperature sense wire is closest to the oven body to minimize the temperature difference between this wire and the sample.

is wound closest to the nickel oven body to reduce the gradient between the sample in the oven and the measured temperature. The temperature is determined from a measurement of the resistance of the platinum wire. The heater wire is wound over the temperature sensing wire.

To prevent electrical contact between the nickel body and the temperature-sensing wire, a thin (0.025-0.05 mm) layer of alumina is coated onto the nickel prior to the winding of the wire. After this wire was wound onto the oven body, another alumina coating was applied to electrically isolate the temperature-sensing and heater wire. A final overcoat of alumina is applied to the heater wire. The alumina affords good thermal conduction between the heater wire and the nickel for effective heat transfer.

Careful reduction of all heat loss mechanisms was necessary to permit calorimetry to be possible to the highest temperatures with the limited power and energy available from the lander. Two thermal radiation shields surround the ovens. One of these is a multiple-layer platinum sheet wrapped around each oven and held in place with a stainless-steel tube. This shield also serves to reduce the heat loss by gas conduction in the 6-mbar atmosphere of Mars because the interlayer distance is less than the mean free path of the atmospheric molecules. The second radiation shield surrounds both ovens and also includes a multiple-layer nickel sheet.

Each male oven pair is mounted on a nickel yoke attached to a flexible bellows that receives carrier gas from the gas-handling system. The bellows is restrained during the vibration of launch by a capture device that is released when the oven is closed. The yoke is attached to the wall of the thermal analyzer housing by two bearings. One of these is free to rotate; the other moves in a milled arc (Figure 2). Under the influence of a drive rod from a wax motor, the yoke is forced to rotate until the bearing in the arc reaches a linear track, whereupon it is driven by a spring to mate the male and female oven halves.

4.2. Gas-Handling System

The TEGA gas-handling system distributes carrier gas or calibration gas and regulates the pressure in the system. The supply tanks have sufficient capacity to support all eight DSC samples with a margin of ~100%. The carrier and calibration gases are distributed to the ovens via a manifold assembly. The manifold contains 19 valves, a pressure sensor, and three flow-regulating frits (Figure 4).

The calibration tank contains nitrogen (60.2%), carbon dioxide (39.8%), water (1 mL of liquid), and oxygen (27 ppm). The water was added to the tank as a liquid so that the gas would be saturated at the tank temperature. In operation, we will control the temperature of the tank to determine the partial pressure of water vapor in the calibration gas supply.

The manifold is highly adaptable in its operation. The oven inlet and outlet valves are operated independently, so it is possible to seal the ovens, flow carrier gas through the ovens, or allow the ovens to vent via the vapor pressure of the evolved gases. The manifold also has a bypass valve which permits calibration gas to be analyzed in the EGA and allows the calibration gas to be purged from the system by flowing carrier gas directly into the EGA before a sample is analyzed. Owing to mass and volume constraints, commercially available, elastomer-sealed, normally closed solenoid valves were selected and qualified for TEGA. The leak integrity of the carrier and calibration supply tanks is maintained by nickel foils which are punctured by a wax-motor mechanism just prior to the first analysis on the surface. The carrier or calibration master valve is pulsed to regulate the pressure of the carrier and calibration gases in the manifold to control the flow rate through the system. At our nominal flow rate of 0.4 standard mL/min the pressure in the oven and oxygen cell is ~120 mbar, and the pressure in the TDL cell is about 10 mbar. These pressures are a function of the flow rate and are determined by various flow restrictors.

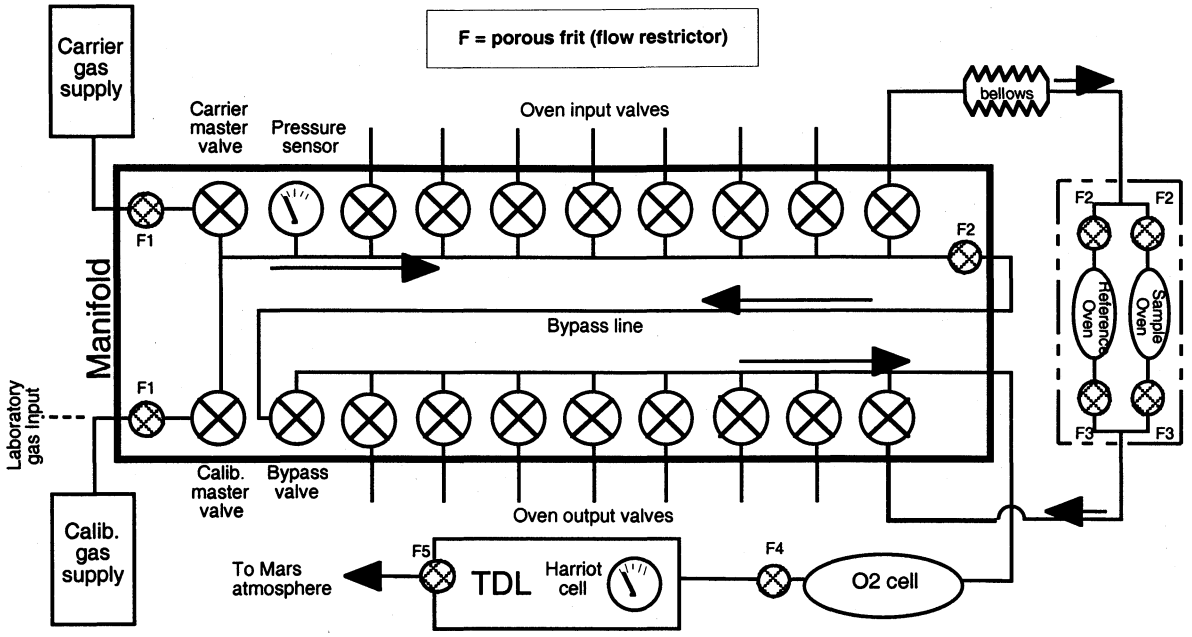

Figure 4. TEGA gas-handling system. Actuation of one of the master valves determines whether carrier or calibration gas is introduced into the system. Controlled, cyclic actuation of the master valve serves as a simple regulator of the pressure, which is monitored by the sensor on the manifold. Each oven pair has an inlet and outlet valve to control the flow of gas and a frit at each end to contain the sample. Additional frits are provided as shown to produce different pressures in the EGA cells. The bypass line is used to supply calibration gas to the EGA cells and to purge them following calibration.

4.3. Evolved-Gas Analyzer

The EGA on TEGA consists of two modules, a small cell containing an oxygen sensor and a larger cell containing two tunable-diode laser (TDL) spectrometers. They receive gases evolved from the sample or from the calibration supply via the gas manifold (Figure 4) and permit time-correlated analysis of gas release and calorimetry.

The TDL spectrometer was built and tested by the Jet Propulsion Laboratory (JPL) and is described in detail elsewhere in this issue [*May et al.*, this issue]. It will be described only briefly here. It consists of a Herriott cell with a 1-m path length and two laser diodes, one for H_2O and one for CO_2. The laser output, after attenuation by passage through the gas in the Herriott cell, is detected by the photodiodes, one for each compound.

Normally, a TDL spectrometer would have the capability of precise alignment of the lasers, but with this system the lasers can only be crudely aligned. The poor alignment gives rise to many optical fringes in the spectrum [*May et al.*, this issue] which change in position from spectrum to spectrum with small changes in temperature. This problem is not so severe that it will compromise our ability to determine the concentration of water or carbon dioxide, but it will compromise our ability to determine the $^{13}C/^{12}C$ ratio in the carbon dioxide release.

The H_2O laser is scanned over the range of 7306.0 cm^{-1} to 7307.5 cm^{-1} to observe the absorption line at 7306.75 cm^{-1}. The CO_2 laser is scanned over the range of 4876.7 cm^{-1} to 4878.6 cm^{-1} to observe the absorption line at 4877.03 and 4878.29, for $^{12}CO_2$, and 4877.58, for $^{13}CO_2$.

The TDL Herriott cell was equipped with a Barocap pressure sensor supplied by the Finnish Meteorological Institute. The purpose of the pressure sensor is to allow us to measure the flow rate through the system based on the pressure drop across the exit frit on the Herriott cell (Figure 4). Knowledge of the flow rate is important since the quantity we are interested in determining is the amount of gas released from the sample, which is the product of concentration, flow rate, and time.

The pressure sensor in the Herriott cell was broken during testing, apparently during a helium leak test before delivery from JPL to Arizona, and there was not sufficient time to replace it in the flight unit. The lack of this sensor, however, will not significantly compromise our ability to determine the amount of gas released from the sample. For small amounts of gas released, we can have confidence in our knowledge of flow rate since it is dominated by the flow rate of carrier gas. When there is a large release of gas, for example, when a carbonate decomposes, the spectroscopic line is pressure broadened, and the line width is a reliable measure of total pressure.

The oxygen sensor is a student-built device that was the basis of the Master's thesis of one of us [*Blanchard*, 1998]. The sensor is made of an electrochemical device with an yttria-doped zirconia electrolyte mounted on an alumina substrate. The sensor has an integral platinum heater deposited on the back of the substrate to allow the sensor to operate over the temperature range of 400°C to 600°C.

The oxygen ion conduction through the solid electrolyte, the source of the current, is limited by the amount of gas that can diffuse through the porous solid electrolyte. In this diffusion-limiting mode, theory predicts that the current through the electrolyte should be linearly proportional to the oxygen partial pressure in the gas until the concentration is high enough to saturate the sensor. Laboratory experiments confirm that the device is linear in response from a partial pressure of O_2 of 0.3 mbar to its saturation limit of 3 mbar.

Below 0.3 mbar, however, the sensor response increases with decreasing O_2 concentration, apparently because the electrolyte becomes temporarily unstable (oxygen ions have been lost from the crystal structure) at such severely reduced oxygen partial pressures. In this starved condition the cell exhibits time-dependent behavior and is unable to maintain its linear responsiveness to O_2 variations between 0.3 and 3 mbar.

To prevent starvation, the carrier gas in TEGA contains 3.5 ppm O_2: at the operating pressure of ~100 mbar, this corresponds to 0.35 mbar, or the start of the linear range of the sensor.

The cell containing the oxygen sensor is made of stainless steel and has porous frits at each end. The exit frit on the oxygen-sensor cell serves to lower the pressure from the nominal 100 mbar at the oxygen sensor to the nominal 10 mbar in the TDL cell. The lower pressure in the TDL cell is needed both to reduce pressure broadening of the lines and to increase the flow rate through the cell and thus the resolving time of the TDL spectrometers. The volume of the oxygen cell is 1.6 cm^3, and our nominal flow rate of carrier gas is 0.4 cm^3/min at standard temperature and pressure (STP). With a cell pressure of 100 mbar and an average cell temperature of ~100°C we get a mixing time constant in the cell of 16 s. The TDL cell has a volume of 26 cm^3, a nominal operating temperature of 35°C, and pressure of 10 mbar, yielding a time constant of 32 s.

4.4. Electronics

In order to fit within the tight volume constraints of the electronics, TEGA uses an entirely digital oven-control system. The oven temperature is compared to a preprogrammed ramp by a high-gain analog difference amplifier whose output is digitized 2000 times each second and fed to a control law implemented in the instrument firmware. The control law, in turn, drives a pulse width modulator which controls the oven heater. Temperature error measurements are taken only in the quiet time between oven power pulses to reduce system noise. Each oven independently tracks the preprogrammed ramp, and the temperature and error signals for each oven are downlinked along with the pulse width data.

Because of the wide temperature range of the ovens, the much higher power needs with increasing temperature, and the increasing resistance of the platinum heaters with temperature, multiple oven-drive voltages of 10 V, 15 V, and 30 V are needed to cover the temperature range of -90 to over +950°C. The oven heater voltage is stepped up as the temperature increases so that the control law and pulse width modulator circuits operate within their ideal range of 10% to 70%. These functions are controlled by a dedicated microprocessor running firmware residing in TEGA electronically erasable programmable read-only memory (EEPROM).

Achieving low noise on the sensor outputs was an important design objective. The oxygen sensor has a full scale range of 4 μA, and our noise level is on the order of the least significant bit on the analog to digital (ADC), 0.2 nA. The temperature sensors on the ovens have a range in resistance from 23Ω to 150Ω over the range from -90 to +950°C. Changes in resistance are sensed by reading the voltage drop over the sense wires, which ranges from 0.23 V to 1.50 V when excited by a constant current source of 10 mA. The voltage noise on this voltage is ~160 μV, also comparable to the least significant bit on the ADC, and this noise translates to a temperature noise of 0.12 K near 0°C. Considering that the sense wire is embedded in a common ceramic and wound on an oven core only a few tens of micrometers from a heater wire that is pulse width modulated with a 30-V heater supply, it may be appreciated that this noise value was difficult to achieve.

The TDL spectrometers use analog electronics identical to those used for the MET TDL spectrometer and are described in detail by *May et al.* [this issue]. The output of the analog electronics is digitized by the same 14-bit ADC used by TEGA to collect all the other science and engineering data. The spectra from both the water and the carbon dioxide spectrometers are collected simultaneously. Each spectrum takes 2.7 s to sweep the wavelength region. During this time the ADC takes 900 samples of each of five analog outputs: water DC power, water 2*f* signal, high-gain water 2*f* signal, carbon dioxide DC power, and carbon dioxide 2*f* signal. The five channels are each cyclically sampled at a rate of 330 Hz to collect all the data within the 2.7-s sweep time.

4.5. Flight Software

The TEGA flight software is a small but important part on the software running on the central lander computer. The lander software is made up of a number of tasks running under version 5.2 of the VxWorks operating system on a lander-provided Power PC single-board computer. This software controls most of the various instruments in the MVACS mission through bidirectional 9600 baud RS422 communication ports on a payload and attitude control interface (PACI) card. TEGA uses one of the ports to communicate with the TEGA microelectronics board/hardware.

The TEGA lander software controls the TEGA microelectronics by interpreting message commands from the MVACS payload coordinator software, formatting and sending commands to the TEGA hardware, receiving and buffering responses and data from the hardware, optionally compressing the data, and then sending them to the telemetry data stream for downlink to Earth.

4.6. Distinctions Between TEGA and a Commercial DSC

As if often the case with a flight instrument, many design compromises were necessary to permit the TEGA instrument to operate remotely in the Martian environment. These compromises led to capabilities different from those normally expected in a laboratory DSC. In some cases the instrument performs better, but in most cases it cannot perform as well. In this section we describe these differences.

4.6.1. Inability to determine an empty-oven baseline. In a commercial DSC, reusable, carefully matched sample and reference ovens allow a baseline measurement of any differences in heat capacity or thermal losses between the sample and reference ovens to be made by performing a DSC analysis with an empty sample oven. Because the ovens in TEGA are launched in an open configuration, they are not in the correct thermal configuration for a baseline determination to be made before the addition of a sample. We also could not afford the complexity, mass, and cost of reusable or multiple-use ovens. Multiple-use ovens would require the ability to add a sample, make a gas-tight seal, perform an analysis, break the seal, and completely remove the sample to prepare for a second sample.

4.6.2. Lack of knowledge of sample mass. We have no means of determining the mass of the sample, so our quantitative determinations will be of ratios of constituents to each other.

4.6.3. Differences in sample environment. In order to minimize the size of the carrier and calibration gas supply tanks, the pressure and flow rate of carrier gas in the ovens is lower than the values typically used in laboratory DSC work, which are

typically conducted at atmospheric pressure and 20 mL/min flow rate. As noted earlier, the transition temperature of reactions that evolve gas is a function of the partial pressure of the evolved gas and is thus affected by the pressure and flow rate of the carrier gas. This difference is not expected to degrade performance relative to a laboratory DSC, but it will yield data with lower transition temperatures than literature values.

4.6.4. Greater temperature range of operation. One advantage of TEGA over a commercial DSC is that we can operate up to higher temperatures. Commercial DSC instruments are usually limited to temperatures on the order of 750°C due to selection of materials. In this case we could afford to develop an expensive high-temperature ceramic that can provide reliable electrical insulation between the heater and the temperature-sense wires at high temperatures. Because TEGA needs to detect the decomposition of carbonates, the high-temperature capability was an important requirement. This construction technique would be too expensive for a commercial DSC, for which such high temperatures are usually not necessary.

5. Operations and Data Analysis

The goals of the TEGA measurements are to determine the concentrations of ices, adsorbed volatiles, and volatile-bearing minerals on the surface and in the subsurface units exposed by the Robotic Arm (RA). The RA will dig a trench up to 50 cm deep, and the Robotic Arm Camera (RAC) will be used to look for macroscopic geologic features (like layering), changes in dust/ice ratios, and changes in either the types of ice or dust based on visible properties (albedo, color, textures) [*Keller et al.*, this issue]. On the basis of an integration of RAC observations and measurement capabilities of TEGA, appropriate samples will be selected and delivered to TEGA.

5.1. Overview of Instrument Operation

TEGA will be operated relatively infrequently on Mars. Because we have the capability for only eight samples, we will spread the analyses over the course of the mission, allowing us better educated operation of the instrument and choice of samples. This section will describe how we expect to conduct an analysis on a typical sample, but we expect to modify this plan with experience gained at Mars.

A nominal TEGA run spans 2 days. Instrument warming, EGA calibration, soil acquisition, oven closure, low-temperature scanning calorimetry, and evolved gas analysis take place on the first day. Soil acquisition includes opening a thermal analyzer door, receiving a sample from the robotic arm, vibrating the sample to load it into the oven, autonomously verifying soil delivery, and performing the low-temperature sample analysis. The second-day activities consist of instrument warming and EGA calibration followed by high-temperature scanning calorimetry and evolved gas analysis. The 2-day sequences are not changed once started. Adjustments will be made for the next sample on the basis of knowledge gained from prior samples.

The instrument is versatile in its ability to perform the sample analysis. For example, we have independent control over five different valves in the manifold, allowing the gas evolved from the samples to be swept to the EGA via the carrier gas, to flow to the EGA owing to its own vapor pressure, or to be sealed in the oven. We also can control the flow rate of the carrier gas to sweep the evolved gas away from the sample at different rates. We can change the DSC heating rate over a wide range, which can affect our ability to see different transitions. Transitions that occur over an extended temperature range and are small in enthalpy change can be detected more easily at higher heating rates as the energy is deposited in a shorter period of time. On the other hand, if there are several closely spaced transitions, the ability to separate them is improved at lower heating rates. In addition, because of the finite time response of the EGA, the ability to resolve multiple gas releases is improved at lower heating rates.

Other strategies we can employ in the operation of the instrument have to do with the melting of ice. We intend to stop the flow of carrier gas well before the ice melting point to avoid freeze-drying the sample. The melting of ice may cause a release of oxygen, since the putative strong oxidant in the Martian soil is known to decompose and release oxygen in the presence of water. Because of this fact, we may intentionally forgo the information learned from the ice melting by freeze-drying some samples. If this action avoids the oxygen release, it may cause the oxidant to thermally decompose, which may further constrain its identity.

5.2. Detailed Operational Scenario

After turn on, the instrument is loaded with parameters that control the engineering data collection rates and begin to warm the instrument. Subsystems which require warming include the manifold, the calibration-gas supply tank, the plumbing, the analog electronics box, the oxygen sensor, and the Herriott cell of the TDL spectrometers. We will also begin to collect science data from the EGA as the instrument warms.

While the instrument is being warmed, it will receive its sample from the robotic arm and load it into the oven. First, one of the eight thermal analyzers is selected, and the doors are opened to permit access to the soil-loading funnel. The robotic arm acquires the sample and delivers it to TEGA, dumping it about 15-20 cm above the selected analyzer. The soil-loading impeller and vibrator is actuated at various programmable frequencies for a period of ~5 min. During this time the instrument is continuously monitoring the oven-fill light-emitting diode to determine if the oven is full. If not, TEGA can autonomously issue a command to the robotic arm to request another sample. This process can continue for a preset maximum number of deliveries, after which, if there is no indication of a full oven, the instrument will shut down and wait for ground command.

Once the instrument is up to operating temperature, we will conduct a calibration of the EGA. The calibration will begin with purging any Mars atmosphere from the EGA with pure carrier gas. After the EGA is purged, the calibration gas will be turned on and flowed through the EGA. We can control the flow rate of the calibration gas, which affects the pressures in the cells, and we can change the temperature of the calibration gas tank, which controls the water content of the calibration gas. As mentioned above, the calibration tank is saturated with water, so the partial pressure of water in the tank is controlled by the tank temperature, which determines the vapor pressure of the water or ice.

After the calibration is over and the EGA has been flushed with carrier gas, the sample analysis begins by flowing carrier gas over the sample to remove interstitial atmosphere. The bypass valve is closed and the oven inlet and outlet valves are opened. The carrier-gas master valve is opened and its duty cycle is controlled to regulate the manifold pressure for the desired flow

Table 2. Determining the DSC Temperature and Power From the Measurements Reported by the TEGA Instrument

Resultant Data	Data Reported by TEGA	Conversion Method
Commanded or ramp temperature	DAC value corresponding to the commanded or ramp temperature	Convert the reported DAC counts to a resistance and then convert the resistance to a temperature.
Measured oven temperature	Voltage drop across platinum temperature sense wires of the sample and reference ovens reported as ADC counts	Convert the reported ADC counts to a resistance and then convert the resistance to a temperature. This calculation relies on an accurate knowledge of the resistance of the sense wire at 0°C.
Power delivered to the sample and reference ovens	Duty cycle of the heater voltage applied to the platinum heater wire of the sample and reference ovens	Use the duty cycle and heater voltage with a calculated value for the heater resistance to calculate a power.
		The heater resistance temperature is determined from the platinum-resistance temperature curve using the sense wire temperature.
	Nominal heater voltage	The heater voltage is determined from the nominal heater voltage as modified by the voltage flag.
	Voltage flag reporting occurrence time of events that affect heater voltage	This calculation relies on an accurate knowledge of the resistances of the sense wire and the heater wire at 0°C.

rate through the system. After ~5 min to flush the oven, the oven heating then begins with a ramp from ambient conditions up to 10°C. At an oven temperature of about -5°C the carrier-gas master valve is closed, cutting off the flow of carrier gas but allowing the oven to vent through the EGA. Any ice that is present is melted, and the melting enthalpy is determined. The sample is then allowed to cool, and the water will freeze. The ovens are ramped up again to ~50°C, and any water is allowed to evaporate. After a predetermined time period for evaporation the flow of carrier gas is resumed, and the oven ramp is continued up to 400°C. The ovens are then held at this temperature for 5 min and then ramped back down to ambient at 20 K/min.

After the oven ramping is done, another purge and calibration cycle is completed. Finally, the manifold is allowed to vent to Mars ambient, and then the valves are closed to allow monitoring of leaks in the master valves by monitoring changes in the manifold pressure overnight.

The second day of the 2-day operation begins with instrument turn on, parameter loading, and instrument warm up. No soil-handling operations are necessary, as the sample is already sealed in the oven from the previous day.

Once the instrument is up to operating temperature, we will again conduct a calibration of the EGA. After the calibration the EGA is flushed with carrier gas, and the sample analysis begins by flowing gas over the sample to remove interstitial atmosphere. After ~5 min to flush the oven, the oven heating then begins with a ramp from ambient conditions up to the maximum temperature (950°C). The ovens are then held at this temperature for 5 min and then ramped back down to ambient at 20 K/min. After the oven ramping is done, another purge and calibration cycle is completed.

5.3. Data Reduction

Unlike laboratory DSC instruments, which are designed to provide only the smoothed differential power and the temperature as an output, the TEGA instrument returns a rich set of fundamental DSC measurements and engineering data from which the temperatures and power must be derived. The reduction of these data to DSC time and temperature series suitable for analysis is briefly summarized in Table 2. Data reduction is complicated by the fact that the applied heater voltage is a function not only of the nominal power supply tap required (either 10, 15, or 30 V) but of the effects of the manifold heater and the TDL blanket heater on the voltage provided by the power supply.

The calculations required to convert the TDL spectral data to molecular number density have been described by *May* [1998] and will only be summarized here. The TDL operates as a Beer-Lambert absorption spectrometer for H_2O and CO_2 utilizing separate lasers and detection systems sharing the same cell. Beer's law of absorption is described by equation (1):

$$I(\nu)/I_0(\nu) = e^{-[\kappa(\nu)L\rho]} \quad (1)$$

where I is the measured intensity at frequency ν, I_0 is the original intensity, L is the optical path length, ρ is the number density, and κ is the absorption coefficient, which depends on the molecular line strength and line shape for the transition under study as well as the laser frequency.

As each laser is swept in frequency over a narrow range, the absorption of laser energy, I_0-I, is detected. The laser frequency is swept linearly with time with a fixed period of 2.7 s. In addition, a sinusoidal modulation frequency f is superimposed on the linear laser frequency ramp to permit phase-sensitive detection through the demodulation of this signal at twice the modulation frequency ($2f$) using the method of a lock-in amplifier.

The peak-to-peak amplitude of the resulting $2f$ spectrum (Figure 5) is then directly related to the number density through relationship (1). Conversion to number density requires a knowledge of the modulation amplitude, which is set during testing, and the absorption coefficient κ, which is a function of the temperature and pressure of the gas. This function is determined by direct measurement in the laboratory and the results are used to build a discrete matrix of values in the range of interest, which is then used by the data reduction software together with a knowledge of the pressure and temperature of the TEGA Herriott cell.

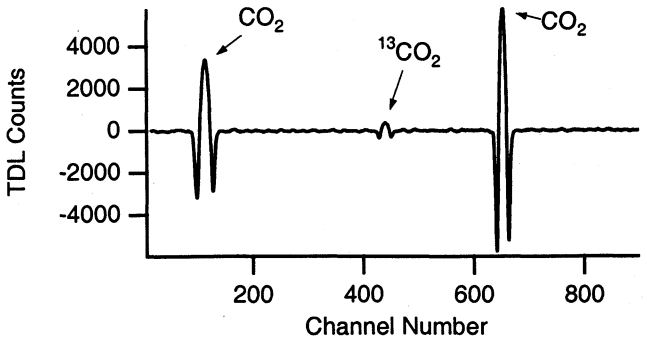

Figure 5. The 2f spectrum of the FM CO_2 TDL illustrating the relative signal strengths of the $^{12}CO_2$ and $^{13}CO_2$ lines. For this spectrum, pure CO_2 was flowing in the TDL cell with the terrestrial ratio of $^{13}CO_2$ to $^{12}CO_2$.

On Mars we expect to always have a small background signal in the TDL spectrometers owing to atmospheric carbon dioxide being in the laser path outside the Herriott cell. In addition, because our sensitivity for water is so high, we expect to see a water signal, presumably from water absorbed on surfaces in the plumbing. We shall determine this background level before and after each run by analyzing the pure carrier gas, which contains no water or carbon dioxide, and subtracting this amount from the value measured during a sample analysis.

Though the calibration gas will be used to calibrate and condition the oxygen sensor, if the sensor is not in its oxygen-starved state (section 4.3), it is needed mainly for the determination of the isotopic composition of the carbon dioxide. Because we cannot be sure that the optical fringes are in exactly the same place in the spectrum at any time, we cannot be sure if they are adding to or subtracting from the signal. By having a fixed composition gas which can be analyzed repeatedly, we can determine our on-Mars ability to reproducibly determine the $^{13}C/^{12}C$ ratio in the calibration gas. The measured ratio will then be normalized to the ratio determined in the calibration gas. The collection of all the measurements of the isotopic composition of the calibration gas at the end of the mission will be used to estimate the reproducibility of the isotopic composition. The effect of the fringes on the strong lines of water and carbon dioxide are small enough that they will have no significant effect on our ability to determine the amount of these compounds released from the sample.

6. Anticipated Results

The complexity of the TEGA instrument has required an extensive calibration and characterization program that is ongoing at the time of this publication and will continue after landed operations. The scale of this effort during instrument development was conditioned by the realities of the funding and time available, both of which were strictly limited.

Tests were conducted on the flight model (FM) to characterize the gas-handling system, the open-oven DSC response, and the TDL spectrometers and oxygen sensor performance using laboratory gases attached to a port on the manifold. Flowing laboratory gas also allowed the measurement of the flow rate through the plumbing system as a function of pressure and temperature and the verification of the pressure regulation system. Test gases were introduced and detected in the oxygen sensor and the TDL. Because of the single-use nature of the TEGA DSC, all calorimetry calibrations have been conducted on the engineering qualification model (EQM), which has thermal analyzer modules identical to the flight unit. All calibration and characterization tests were conducted in a Mars environmental chamber operated at 6-mbar nitrogen or CO_2 pressure and variable ambient temperatures.

6.1. Calibration and Performance

After the DSC data are converted into temperature and power, the calibration of the TEGA DSC is similar to that of any DSC. For a detailed discussion of these issues, see *Höhne et al.* [1996]. These are principally (1) temperature calibration, which establishes the relationship between the measured temperature and the temperature of transition of pure substances, such as melting of indium, and (2) enthalpy calibration, which establishes the relationship between the measured enthalpy change and the known transition enthalpy change of pure substances.

The melting of water, gallium, indium, aluminum, and lithium sulfate were used for temperature and enthalpy calibration because they span the temperature range of interest and are reversible (allowing multiple determinations for a single oven load). They also have well-defined, unambiguous transition peaks.

The determination of the transition onset temperature and enthalpy for a low-temperature pure substance (15 mg of indium) is illustrated in Figure 6. The ramp rate for this run was 5.35 K/min. The differential power is plotted against the temperature after subtraction of a polynominal fit to the baseline. The observed onset temperature is determined by fitting a straight line from the peak maximum to the rising edge of the peak and noting the intercept with the axis. In the case shown the onset temperature is observed to occur at 157.5°C compared to a known value of 156.6°C.

Figure 6 shows a large amount of noise typical of most of our early calibration studies. After delivery of the instrument, however, we found that we were able to significantly improve the control law stored in the instrument firmware. The noise performance following optimization is nearly an order of magnitude better than that of the delivered firmware. The firmware in the flight instrument will be reprogrammed to deliver this low-noise performance.

Performance of the DSC at temperatures above 300°C, before control law optimization, is shown in Figure 7 for a run with 4.1 mg of fully hydrated lithium sulfate and 2.9 mg of aluminum heated at a ramp rate of 20.4 K/min. These data, when scaled for differences in reaction enthalpies, imply a minimum detectable calcite decomposition of ~0.14 mg, or 0.5% of a 30-mg sample, a result consistent with the geologic sample run with calcite reported below. Calcite displays a broad peak but has a large heat of transition (1670 J/gm). Other carbonates have broad peaks and smaller transition enthalpies and will be detectable at lower sensitivities. The coincident observation of CO_2 in the TDL will provide an unambiguous determination of carbonate decomposition. A test of the system with water present is shown in Figure 8. The sample contained 10 mg of water added to an inert alumina substrate. The ice-melting and water-evaporation endothermic peaks are readily observed (Figure 8). Analysis of this test indicates a melting detection threshold of water ice in the

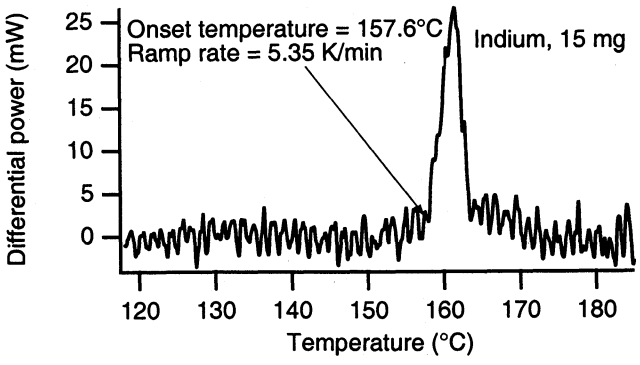

Figure 6. Determination of the onset temperature and the enthalpy for a pure sample as illustrated by a TEGA EQM run with a 15 mg sample of indium. The onset temperature is defined as the intersection of the baseline and a straightline fit to the leading edge of the peak. The enthalpy change of the sample corresponds to the area of the peak when power is plotted against time. The noisy data are due to a nonoptimized control law (see text).

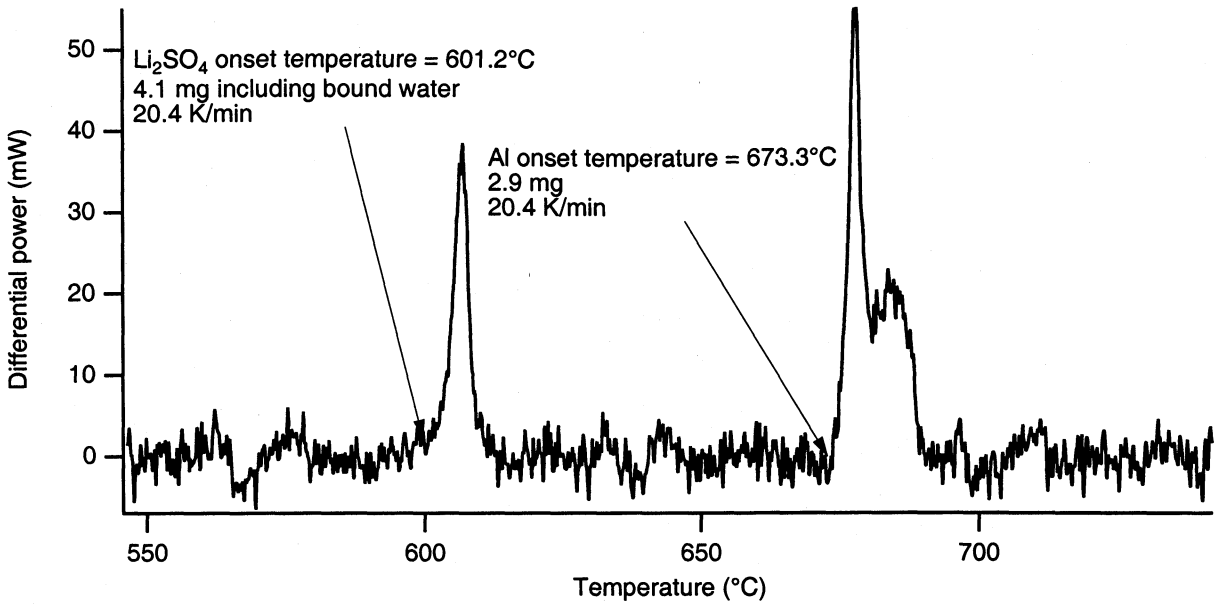

Figure 7. Calibration run with lithium sulfate and aluminum in the TEGA EQM. This run and the indium run were used to establish the temperature and caloric calibration of the TEGA DSC. The noisy data are due to a nonoptimized control law (see text).

sample of better than 0.2% by mass, assuming a typical oven load of 30 mg.

In order to assess our ability to detect carbon dioxide and water over the background signals mentioned in section 5.3, we collected data with just carrier gas flowing through the Herriott cell. The ambient atmosphere in the instrument test chamber was 7 mbar of CO_2 to simulate the Mars atmosphere. We collected sufficient data to calculate a mean and standard deviation on these signals.

The results show that we can detect H_2O at a 3-σ level of 1 μbar and CO_2 at a 3-σ level of 15 μbar. For our standard flow rate of 0.4 std mL/min, a typical release time of 5 min, and a sample mass of 30 mg, these limits translate to the equivalent amounts in the sample of 8 ppm of H_2O and 0.03% of CO_2. For both compounds our sensitivity is clearly much greater than that needed for our scientific problems.

The TDL spectrometers also have the ability to determine the $^{13}C/^{12}C$ ratio in evolved CO_2 via a weak absorption line for ^{13}C.

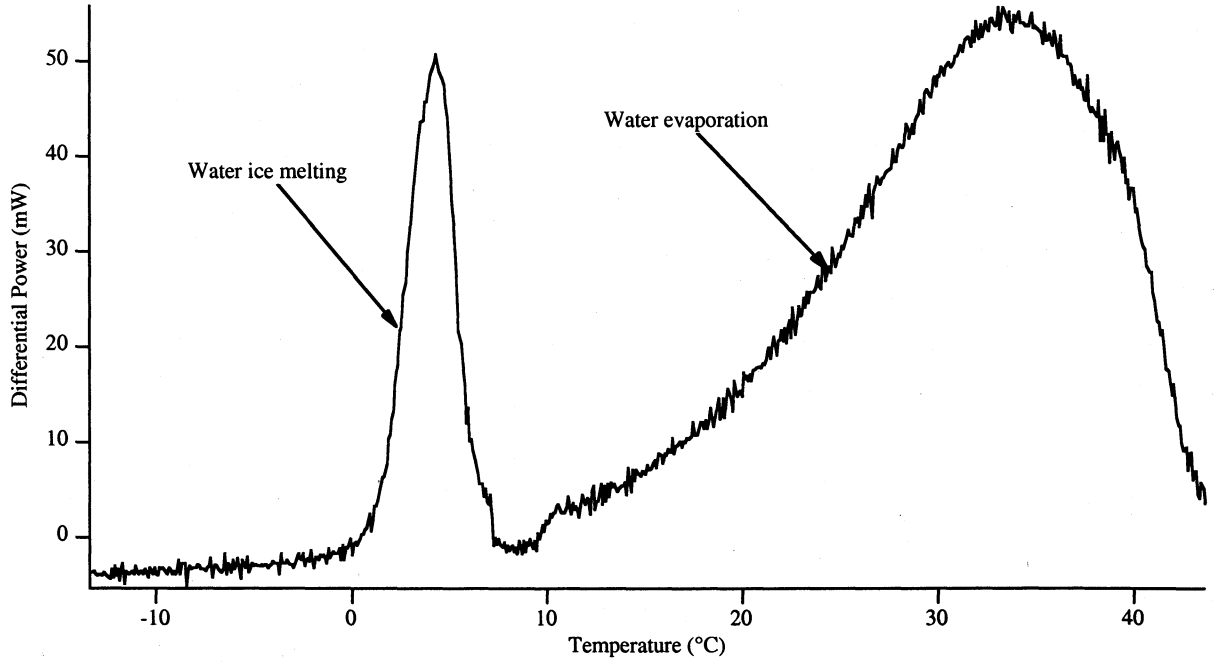

Figure 8. The melting and evaporation of 10 mg of water was observed in an end-to-end system test. Clear separation between the two processes is observed.

Table 3. Detection Limits and Precision of Important Analysis Parameters

Parameter	Detection Limit/Precision	Limit in 30-mg Sample
Ice (via calorimetry)	0.05 mg	0.2%
Calcite (via calorimetry)	0.14 mg	0.5%
Water vapor (via EGA)	1 μbar	8 ppm
Carbon dioxide (via EGA)	15 μbar	0.03%
Carbon dioxide isotopic ratio[a]	± 0.6 % (precision)	

[a]At constant temperature with little motion of optical fringes

Unfortunately, as mentioned in section 4.3, the TDL spectrometers have degraded performance caused by optical fringes due to difficulties in properly aligning the lasers.

We did some tests to determine the accuracy and precision of these data by flowing pure CO_2 in the Herriott cell. This is not an unrealistic test, as a major release of CO_2 from a carbonate decomposition will provide a comparable partial pressure to that observed with 0.4 std mL/min of CO_2. Under ideal conditions, where the temperature variation of the Herriott cell could be controlled to within 0.03 K, we found a 2-σ precision of 0.6% in the $^{13}C/^{12}C$ ratio by averaging over a typical carbonate gas-release time of 5 min.

Examination of the multiple spectra taken during this interval show that the fringes were stable and not moving in the spectra. This value of 0.6% is precision, not an accuracy, however, since the position of the fringes can change and affect the result. When we did not take normal precautions for temperature control, we found variations in the $^{13}C/^{12}C$ ratio of 9% (2-σ), and the fringes were clearly moving through the spectra. Because the fringes can sometimes add and sometimes subtract from the signal, our accuracy will be no better than 9% unless we can have confidence that the fringes have not moved from the time we analyze the sample to the time we analyze the calibration gas. Because we expect the CO_2 release to be at high temperatures and near the end of the calorimetry run, we plan to calibrate the TDL spectrometers soon after the gas evolution, possibly before the fringes have drifted. On the other hand, because the local Mars temperature and winds will be changing, we may not be able to control the temperature to the tight tolerance we could achieve in the laboratory. If we find that all of our calibration runs, made on different days over the life of the mission, give results with high precision, we can then have confidence to equate the accuracy to this precision.

A summary of these results is provided in Table 3.

6.2. Analog Materials

We recognize that the identification of unknown mineral transitions may be difficult on the real Martian samples. We may very well find minerals which we did not expect, and because of the low operating pressure and interactions between minerals, the literature data describing the transitions may not always be directly applicable. Thus we have begun a program of testing with candidate analog materials to see what differences we may expect to see with mixtures of minerals evolving gases at low pressures versus single minerals at atmospheric pressures. This effort will continue through landed operations but has begun with two simple samples intended to test the instrument's capability to measure geologic materials.

We have selected a complex Mars analog sample to test in the EQM TEGA. The sample contains a 27-mg mixture of lepidocrocite (γ-FeOOH, 28 wt %), pyrolusite (MnO_2, 4 wt %), and calcite ($CaCO_3$, 28 wt %). Corundum powder was used as an inert filler for the remainder of the sample. This sample is ideal for testing the DSC and the TDL because H_2O, O_2, and CO_2 will be evolved during the heating process. Under standard DSC laboratory operating conditions, lepidocrocite will undergo a

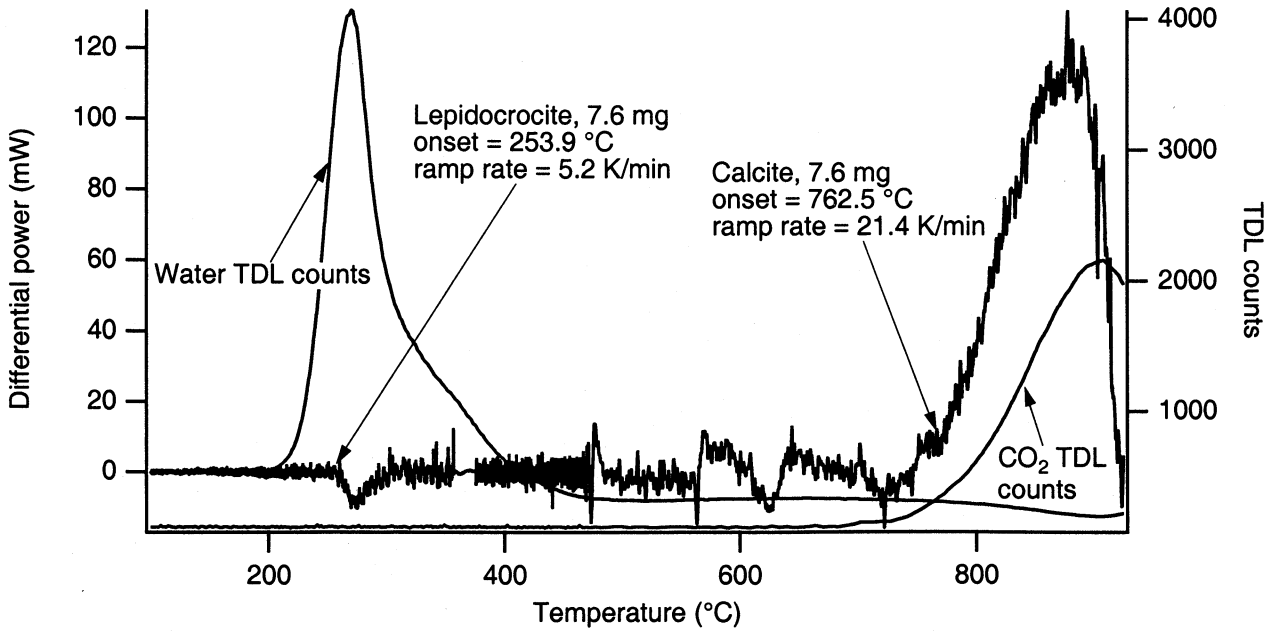

Figure 9. Sample run in the TEGA EQM. Lepidocrocite, pyrolucite, and calcite demonstrate the detection of multiple thermal transitions and their associated gas releases. Lepidocrocite releases water as it transforms into maghemite, and calcite releases CO_2 during its decomposition. The DSC data were taken before we optimized the control law to reduce noise.

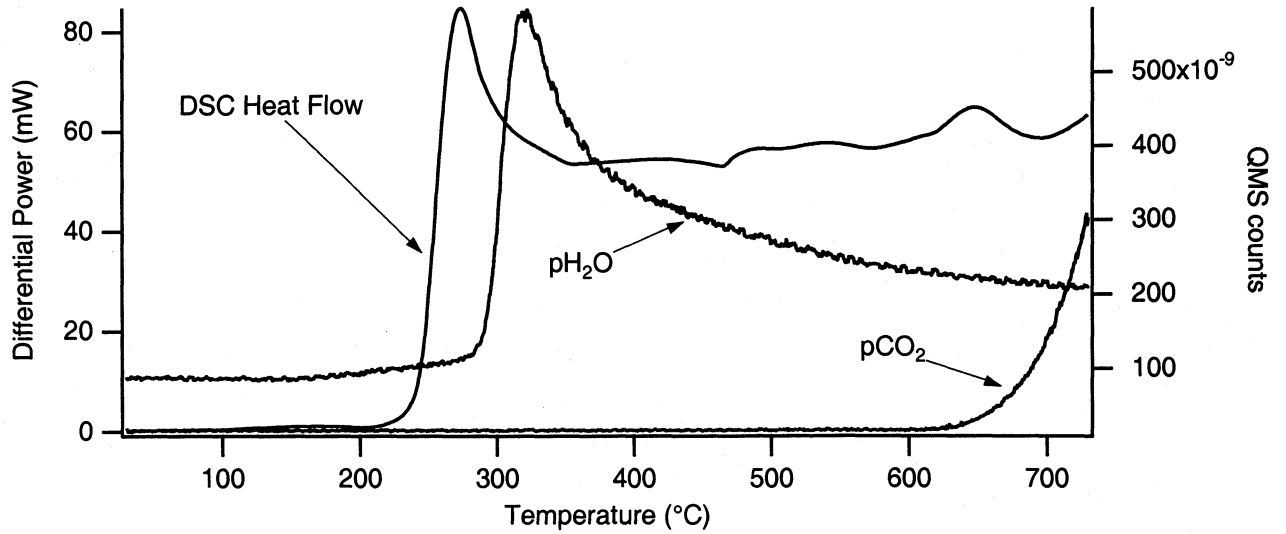

Figure 10. Lepidocrosite, pyrolucite, and calcite sample run in Perkin-Elmer laboratory DSC. Evolved gas detection was performed with a quadrapole mass spectrometer. The full calcite transition occurs at temperatures higher than the maximum instrument temperature.

transformation to maghemite around 260°C as water evolves, and then maghemite transforms to hematite around 420°C. Pyrolusite decomposes into Mn_2O_3 (bixbyite) as O_2 evolves at around 620°C, and CO_2 will evolve around 900°C as calcite decomposes into CaO.

The EQM TEGA experimental run for the analog sample is shown in Figure 9. The lepidocrocite to maghemite transition was clearly detected by the H_2O TDL beginning around 220°C. The DSC onset temperature for the lepidocrocite dehydroxylation endothermic reaction occurred at around 230°C. The CO_2 TDL signature and the strong DSC endothermic peak that begin around 760°C indicate the decomposition of calcite. Because of the reduced pressure operating conditions within the DSC oven, the onset temperature is lower than what would be expected under standard laboratory DSC operating conditions. The DSC responses for the transition of maghemite to hematite and the release of O_2 from the decomposition of pyrolusite were not clearly identified.

For comparison to the EQM TEGA analog sample run, an experimental run with the analog sample was conducted by a laboratory DSC integrated with a quadrupole mass spectrometer (DSC/QMS) (Figure 10). In this run the operating pressure and carrier gas flow rate have been modified to mimic the operating conditions in the EQM TEGA. The DSC onset temperature for the dehydroxylation of lepidocrocite at 248°C is similar to the onset temperature for lepidocrocite dehydroxylation in the EQM TEGA run though there was a delay in the detection of H_2O by the QMS. The difference in the time of gas detection between the EQM TEGA and the laboratory DSC/QMS is due to longer gas lines in the laboratory DSC/QMS. The DSC onset temperatures for the maghemite/hematite transition and pyrolusite decomposition were 473° and 572°C, respectively, for the laboratory DSC/QMS run. Although the upper temperature limit for our laboratory DSC is limited to 725°C, we were able to detect the beginning of CO_2 evolution by the QMS at around 675°C.

7. Summary

The TEGA instrument described herein is capable of addressing many of the important science issues associated with Martian volatiles and climate. We can clearly detect the presence of ice and carbonates, and we can quantify the amounts present. Mixtures of components can be resolved, but we will not know if we can determine the exact minerals present until data are actually acquired at Mars. The synergistic combination of a DSC and an EGA, a combination never before flown, will be a powerful tool for understanding the volatile-bearing phases in the Martian regolith and dust.

Acknowledgments. The authors wish to thank the contributions of many individuals and organizations who contributed significantly to our ability to design, build, test, and deliver the TEGA instrument within the proposed budget. The instrument could not have been built without the hard labor and dedication of the staff of the LPL machine shop, Ron James and Bill Verts, and our electronics support from Rick Schmidt. The management and engineering team at the Jet Propulsion Laboratory were also especially helpful. This group consisted of Young Park, Barry Goldstein, Raul Romero, Mau Tran, David Nakamoto, and David Swenson. The staff at Jackson and Tull in Greenbelt, MD, Mike Cuviello and Phil Gill, who fabricated the electronics boards, were also very helpful and understanding of our deadlines. Local support from our documentarian, Mark Jackson, business manager, Heather Enos, and administrative associate, Glinda Davidson, was also critical in our getting the job done. David Kingery was a very helpful guru on advanced ceramics, a necessary component of our high-temperature ovens, and Mike Fontanarosa was very helpful in design of the field-programmable gate arrays. The support and dedication of many students who worked long and hard to maintain our computer systems (Chris Lewicki), fabricate our ovens (David Burke), construct the electronics (Richard McCord), develop software (Brennan Cropper, Dimitris Papamichail, Amy Mclaughlin, Zoltan Szilagyi, Vinit Deshpande, and Arivu Mani Ramasamy), and to test, test, and test the instrument (Ken Lempke, Gary Quadlander, and David Florkiewicz) are also especially appreciated. The support of numerous people who assisted in the integration and test activities at Lockheed Martin Astronautics (Jeff Slostad and Steve Bailey) is also greatly appreciated.

References

Anderson, D.M., M.J. Schwarz, and A.R. Tics, Water vapor adsorption by sodium montmorillonite at –5C, *Icarus, 34*, 638-644, 1978.

Blanchard, J.A., Specific gas sensing using zirconia amperometric oxygen sensors, MS thesis, Univ. of Ariz., Tucson, 1998.

Blazek, A., *Thermal Analysis*, Van Nostrand Reinhold, New York, 1972.

Bonitz, R.G., et al., Mars Volatiles and Climate Surveyor Robotic Arm, *J. Geophys. Res.*, this issue.

Carr, M.H., Mars: A water-rich planet?, *Icarus, 56*, 187-216, 1986.

Carr, R.H., M.M. Grady, I.P. Wright, and C.T. Pillinger, Martian

atmospheric carbon dioxide and weathering products in SNC meteorites, *Nature, 314*, 248-250, 1985.

Clayton, R.N., and T.K. Mayeda, Isotopic composition of carbonate in EETA 79001 and its relation to parent body volatiles, *Geochim. Cosmochim. Acta, 52*, 925-927, 1988.

Clifford, S.M., A model for the climatic behavior of water of Mars, Ph. D. thesis, Univ. of Mass., Amherst, 1984.

Clifford, S.M., and D. Hillel, The stability of ground ice in the equatorial regions of Mars. *J. Geophys. Res., 88*, 2456-2474, 1983.

de Bruyn, C.M., and H.W. van der Marel, Mineralogical analysis of soil clays, *Geol. Mijnbouw, 16*, 407-428, 1954.

Fanale, F.P., and W.A. Cannon, Adsorption on the Martian regolith, *Nature, 230*, 502-504, 1971.

Fanale, F.P., and W.A. Cannon, Exchange of adsorbed H_2O and CO_2 between the regolith and atmosphere of Mars caused by changes in surface insolation, *J. Geophys. Res., 79*, 3397-3402, 1974.

Fanale, F.P., and W.A. Cannon, Mars: The role of the regolith in determinig atmospheric pressure and the atmosphere's response to insolation changes, *J. Geophys. Res., 83*, 2321-2325, 1978.

Fanale, F.P., J.R. Salvail, W.B. Banerdt, and R.S. Saunders, Mars: The regolith-atmosphere-cap system and climate change, *Icarus, 50*, 381-407, 1982.

Fanale, F.P., J.R. Salvail, A.P. Zent, and S.E. Postawko, Global distribution and migration of subsurface ice on Mars, *Icarus, 67*, 1-18, 1986.

Fanale, F.P., S.E. Postawko, J.B. Pollack, M.H. Carr, and R.O. Pepin, Mars: Epochal climate change and volatile history, in *Mars*, pp. 1135-1179, chap. 32, Univ. of Ariz. Press, Tucson, 1992.

Francois, L.M., J.C.G. Walker, and W.R. Kuhn, A numerical simulation of climate changes during the obliquity cycle on Mars, *J. Geophys. Res., 95*, 14,761-14,778, 1990.

Golden, D. C., D. W. Ming, H. V. Lauer Jr., R. V. Morris, C. Galindo Jr., and W. V. Boynton, Differential scanning calorimetry of hydrous minerals under Mars-like conditions: Calibration studies for the Mars '98 Lander Thermal and Evolved Gas Analyzer, *Lunar Planet. Sci.* [CD-ROM] *XXX*, abstract 2027, 1999.

Gooding, J.L., J.H. Allton, T.B. Byers, R.P. Dunn, F.L. Gibbons, and D.B. Pate, Thermal analyzer for planetary soils (TAPS) experiment, 2, Water sensors (abstract), *Lunar Planet. Sci., XXIII*, 427-428, 1992a.

Gooding, J.L., R.E. Arvidson, and M.Y. Zolotov, Physical and chemical weathering, in *Mars*, edited by H.H. Kieffer et al., pp. 626-651, Univ. of Ariz. Press, Tucson, 1992b.

Gooding, J.L., A.J. Kettle, and H.V. Lauer Jr., DSC sensitivity to hydrated minerals in planetary samples (abstract), *Lunar Planet. Sci., XXIII*, 463-464, 1994.

Herkenhoff, K.E., and B.M. Murray, High resolution topography and albedo of the south polar layered deposits on Mars, *J. Geophys. Res., 95*, 14,511-14,529, 1990.

Höhne, G., W. Hemminger, H.J. Flammersheim, *Differential Scanning Calorimetery*, Springer-Verlag, New York, 1996.

Jull, A.J.T., C.J. Eastoe, S. Xue, and G.F. Herzog, Isotopic composition of carbonates in the SNC meteorites Allan Hills 84001 and Nakhla, *Meteoritics, 30*, 311-318, 1995.

Keller, H.V., et al., The MVACS Robotic Arm Camera, *J. Geophys. Res.*, this issue.

Klein, H.P., The Viking biological experiments on Mars, *Icarus, 34*, 666-674, 1978.

Leshin, L.A., S. Epstein, and E.M. Stolper, Hydrogen isotope geochemistry of SNC meteorites, *Geochim. Cosmochim. Acta, 60*, 2635-2650, 1996.

May, R.D., Open-path, near-infrared tunable diode laser spectrometer for atmospheric measurements of H_2O, *J. Geophys. Res., 103*, 19,161-19,172, 1998.

May, R.D., S. Forouhar, W.S. Woodward, D.A. Paige, A.V. Pathare, and W.V. Boynton, The MVACS tunable diode laser spectrometers, *J. Geophys. Res.*, this issue.

Mellon, M.T., and B.M. Jakosky, Geographic variations in the thermal and diffusive stability of ground ice on Mars, *J. Geophys. Res., 98*, 3345-3364, 1993.

Mooney, R.W., A.G. Keenan, and L.A. Wood, Adsorption of water vapor by montmorillonite, II, Effect of exchangeable ions and lattice swelling as measured by X-ray diffraction, *J. Am. Chem. Soc., 74*, 1371-1374, 1952.

Paige, D.A., The thermal stability of near-surface ground ice on Mars, *Nature, 356*, 43-45, 1992.

Paige, D.A., and K.D. Keegan, Thermal and albedo mapping of the polar regions of Mars using Viking Thermal Mapper observations, 2, South polar region, *J. Geophys. Res., 99*, 25,993-26,013, 1994.

Robie, R.A., B.S. Hemmingway, and J.R. Fisher, Thermodynamic properties of minerals and related substances at 298.15 K and 1 bar (105 pascals) pressure and at higher temperatures, *U.S. Geol. Surv. Bull.*, 1451, 1978.

Romanek, C.S., M.M. Grady, I.P. Wright, D.W. Mittlefehldt, R.A. Socki, C.T. Pillinger, and E.K. Gibson Jr., Record of fluid-rock interactions on Mars from the meteorite ALH84001, *Nature, 372*, 655-657, 1994.

Smith, D.E., et al., The global topography of Mars and implications for surface evolution, *Science, 284*, 1495-1503, 1999.

Smith, P.H., et al., The MVACS Surface Stereo Imager on Mars Polar Lander, *J. Geophys. Res.*, this issue.

Thomas, P., S. Squyres, K. Herkenhoff, A. Howard, and B. Murray, Polar deposits of Mars, in *Mars*, edited by H.H. Kieffer et al., pp. 767-795, Univ. of Ariz. Press, Tucson, 1992.

Toon, O.B., J.B. Pollack, W. Ward, J.A. Burns, and K. Bilski, The astronomical theory of climatic change on Mars, *Icarus, 44*, 552-607, 1980.

Vadavada, A.R., J.-P. Williams, D.A. Paige, K.E. Herkenhoff, N.T. Bridges, R. Greeley, B.C. Murray, D.S. Bass, and K.S. McBride, Surface properties of Mars' polar layered deposits and Polar Lander sites, *J. Geophys. Res., 105*, 6961-6969, 2000.

Williams, M.S., W.V Boynton, R.L. James, W.T. Verts, S.H. Bailey, D.K. Hamara, Thermal and Evolved Gas Analyzer, paper presented at 32nd Mechanism Conference, Kennedy Space Center, Cape Canaveral, Florida, 1998.

Wright, I.P., R.H. Carr, and C.T. Pillinger, Carbon abundance and isotopic studies of Shergotty and other shergottite meteorites, *Geochim. Cosmochim. Acta, 50*, 983-991, 1986.

Wright, I.P., M.M. Grady, and C.T. Pillinger, Chassigny and the nakhlites: Carbon-bearing components and their relationship to Martian environmental conditions, *Geochim. Cosmochim. Acta, 56*, 817-826, 1992.

Zent, A.P., On the thickness of the oxidized layer of the Martian regolith, *J. Goephys. Res., 103*, 31,491-31,498, 1998.

Zent, A.P., and C.P. McKay, The chemical reactivity of the Martian soil and implications for future missions, *Icarus, 108*, 146-157, 1994.

Zent, A.P., and R.C. Quinn, Simultaneous adsorption of CO_2 and H_2O under Mars-like conditions and applications to the evolution of the Martian climate, *J. Goephys. Res., 100*, 5341-5349, 1995.

Zent, A.P., F.P. Fanale, J.R. Salvail, and S.E. Postawko, Distribution and state of H_2O in the high-latitude shallow subsurface of Mars, *Icarus, 67*, 19-36, 1986.

Zent, A.P., F.P. Fanale, and S.E. Postawko, Carbon dioxide: Adsorption on plagonite and partitioning in the Martian regolith, *Icarus, 71*, 241-249, 1987.

Zuber, M.T., et al., Observation of the north polar region of Mars from the Mars Orbiter Laser Altimeter, *Science, 282*, 2053-2060, 1998.

W.V. Boynton, S.H. Bailey, J.A. Blanchard, R.C. Bode, W.R. Fitzgibbon, D.K. Hamara, K.E. Kerry, W. Ko, D.A. Kring, R.D.Lorenz, K.R. Sridhar, M.G.Ward, and M.S. Williams, Lunar and Planetary Laboratory, Department of Planetary Sciences, University of Arizona, Space Sciences Building, Tucson, AZ 85721. (wboynton@lpl.arizona.edu)

D.C. Golden, H.V. Lauer Jr., and D.W. Ming, Johnson Space Center, Houston, TX.

L.A. Leshin, Department of Geology, Arizona State University, Tempe, AZ.

R.D. May, Jet Propulsion Laboratory, California Institute of Technology, Pasadena, CA.

D.A. Paige and A.V. Pathare, Department of Earth and Space Sciences, University of California, Loas Angeles, CA.

R.C. Quinn and A.P. Zent, Ames Research Center, Moffett Field, CA.

(Received July 30, 2000; revised September 27, 2000; accepted October 12, 2000.)